Electric Power Systems Research 214 (2023) 108842

Contents lists available at ScienceDirect

Electric Power Systems Research

journal homepage: www.elsevier.com/locate/epsr

Energy management in DC microgrid with an efficient voltage compensation mechanism

Md. Shafiul Alam [a,*], Fahad Saleh Al-Ismail [a,b,c,d], Fahad A. Al-Sulaiman [b,c], Mohammad. A. Abido [b,c,d]

[a] Applied Research Center for Environment & Marine Studies (ARCEMS), King Fahd University of Petroleum & Minerals, Dhahran, Saudi Arabia
[b] K.A.CARE Energy Research & Innovation Center (ERIC), King Fahd University of Petroleum & Minerals, Dhahran, Saudi Arabia
[c] Interdisciplinary Research Center of Renewable Energy and Power Systems (IRC-REPS), King Fahd University of Petroleum & Minerals, Dhahran, Saudi Arabia
[d] Department of Electrical Engineering, King Fahd University of Petroleum & Minerals, Dhahran, Saudi Arabia

ARTICLE INFO

Keywords:
Direct current (DC) microgrid
State of charge
Energy storage system
Supercapacitor and battery
Fractional-order voltage compensation
Small-signal model

ABSTRACT

Direct current (DC) microgrid facilitates the integration of renewable energy sources as a form of distributed generators (DGs), DC loads, and energy storage system (ESS) devices. A new voltage compensation mechanism is presented in this study to resolve the control issues of DC microgrid in a distributed manner. In this mechanism, a fractional-order voltage compensation term is used in the outer controller loop which eliminates the voltage deviation in the steady-state condition. A detailed mathematical model is developed for the ESS along with the new voltage compensation controller to facilitate proper tuning of the control parameters. Since the proposed voltage compensation term guarantees autonomous bus voltage restoration, the supercapacitor state of charge (SoC) remains at nominal value without violation while it only buffers fluctuating power. However, the battery only compensates for the nominal power demand. The DG power control algorithm strictly maintains the battery SoC within lower and upper bounds. A DC microgrid comprising hybrid ESS, DC load, constant power load (CPL), and distributed generator is implemented with real time digital simulator (RTDS). The results show that the proposed controller is reliable, leading to excellent ESS performance and power management within the microgrid, without any DC bus voltage deviation.

1. Introduction

Over the last few decades, due to the increased global population and industrialization, the energy demand has been increased manifold. As a result, huge energy generation from fossil fuels has created several environmental problems. In order to mitigate the environmental issues and meet increased energy demand, renewable energy (RE) has gained more attention. However, several technical issues, such as uncertainty, complex control, less reliability, low inertia, fault ride through capability, and reserve capacity have arisen due to RE integration [1,2]. The DC microgrid has great capability to facilitate RE integration in the form of the distributed generator (DG). The DC microgrid offers several benefits in DG integration compared to AC microgrid such as solar photovoltaic (PV) connection to the DC bus without any inverter, direct connection of DC loads to the DC bus, and no reactive power and frequency control issues [3,4].

In general, the control of DG and ESS units in DC microgrid has two main objectives such as bus voltage control and load power-sharing [5,6]. The former targets to regulate DC bus voltage without any deviation in steady-state condition while the latter targets to properly manage load-sharing among the DGs depending on their capability and availability [7]. To achieve these control goals, the most widely used technique is the decentralized droop technique. However, in the traditional droop control approach, there always exists a trade-off since the two objectives cannot be fulfilled in the presence of uncertainty with the line parameters [8,9]. Moreover, improper selection/design of droop control parameters may be responsible for inaccurate power-sharing and DC link voltage deviation. As a result, centralized controllers with low bandwidth communications links are offered in many literature [10–12]. It is noteworthy that the DC microgrid integrates many energy storage devices (ESSs) including both the supercapacitor and battery to improve the reliability of the supply system. Therefore, the droop controller design should consider the state of charge (SoC) to protect ESS from over-charging and under-discharging. However, due to droop parameters variations, the

* Corresponding author.
E-mail address: mdshafiul.alam@kfupm.edu.sa (M.S. Alam).

https://doi.org/10.1016/j.epsr.2022.108842
Received 14 March 2022; Received in revised form 13 August 2022; Accepted 26 September 2022
Available online 13 October 2022

Table 1
Comparison of the existing literature.

Methods	Advantages	Disadvantages
Decentralized droop control [7,8]	Simplest control without communication	Tradeoff between voltage control and power-sharing Line parameters uncertainty degrades performance
Centralized control [10–12]	Accurate voltage control and power-sharing	Less reliability Chance of single point failure
Distributed control [16,40,41]	Only neighboring communications are needed Plug and Play capability	High communication complexity
Hierarchical control [42]	Voltage control and load-sharing are improved Low bandwidth communication can be used	Control levels (primary, secondary, tertiary) increase complexity
Consensus-based control [43,44]	Communications are needed only for some ESS devices Improved power-sharing	It needs continuous information transfer

full output power control of ESS cannot be guaranteed. Therefore, advanced control approaches are needed to design to achieve accurate power-sharing while considering the SoC of ESS.

In [13], a centralized approach is presented to achieve accurate power-sharing and satisfactory DC bus voltage control. However, such a communication-based centralized hierarchical control approach has less reliability as it is susceptible to the single point failure [14,15]. Therefore, the reliability of the DC microgrid can be improved with the sparse communication-based distributed control algorithms [16–18]. The power-sharing and voltage regulation can be achieved by voltage regulation terms, processed by the proportional-integral (PI) controllers, which are added to the conventional droop controller [16]. Nevertheless, these control approaches [13,16–19] face large-signal stability problems.

Another important issue in DC microgrid control is that different ESSs have different energy storage properties; for example, the battery has high energy density while the supercapacitor has high power density [20,21]. The battery has a slow response and is suitable to provide constant loads at steady-state while the supercapacitor has a fast response and is effective to shave the peak power in DC microgrid [22]. Therefore, an efficient control approach with hybridization of ESS in DC microgrid can mitigate frequent charging and discharging of batteries, and improve lifetime by minimizing the depth of discharge (DoD) [23,24]. In order to exploit the advantages of hybrid ESS, several control approaches such as filter-based approach [25,26], droop method [27,28], optimization approach [29,30], model predictive control [31,32] are presented. However, since the DC microgrid is distributed in nature, without communication or with less communication link-based decentralized control approaches are more suitable.

Although the power-sharing in hybrid ESS system is improved with the modified droop controller [33], accurate sharing is not achieved. The improvement in power-sharing is also achieved by virtual resistance and virtual impedance droop controllers [34]. Another power-sharing approach is presented in [35] for hybrid battery and supercapacitor system to improve the DC bus voltage deviation. However, this approach uses a conventional proportional derivative (PI) controller and requires bus voltage information exchange between the battery and supercapacitor. In general, virtual resistance droop controller is used for homogeneous ESS devices and impedance droop controller is applied for heterogeneous ESS devices [36,37]. A combined virtual resistance and capacitance droop is applied [37] to provide different frequency components of loads by different ESS devices. However, accurate load sharing is not yet achieved due to the fact that primary level control is not sufficient for energy balancing and load sharing. In [38], energy management and load sharing for hybrid ESS by virtual impedance droop-based distributed controller is presented. However, this approach requires communication links among the ESS devices. In [39], energy management and SoC balancing in DC microgrid is presented which is not suitable for hybrid ESS as droop parameters are considered as a time-constant of filter-based approach which could result in inefficient power-sharing. A comarison of the existing contorl methods is provided in Table 1.

According to the above-mentioned gaps and their importances, this paper proposes a distributed control approach with minimum communication for DC microgrid comprising hybrid ESS. A fractional-order voltage compensation is introduced in the outer control loop and a detailed small-signal model is derived to facilitate controller parameter tuning. An optimization algorithm is applied for the developed small-signal model in order to minimize the integral square error. The cooperation of the voltage compensation mechanism and capacitive droop helps allocate transient parts of the load power to the battery and steady-state parts to supercapacitor while the DC bus voltage is strictly maintained to the nominal value. As compared to the conventional integer-order voltage compensation, the proposed fractional-order compensation guarantees stable and robust operations due to the higher degree of freedom. In addition to strict voltage regulation and power allocation, a rule-based non-complex power sharing and SoC balancing algorithms are developed. The DC microgrid also consists of distributed generators, constant power load (CPL), AC loads with the inverter, and resistive loads. Different load variations are executed to validate the performance of the proposed controller in terms of accurate power sharing and voltage control capabilities. The DC microgrid and its controllers are implemented in real time digital simulator (RTDS) based platform. The main features of the proposed approach are listed below.

- The strict DC voltage regulation is achieved due to the fractional-order voltage shifting term. The bus voltage returns to its reference value immediately after any disturbances. The load or generation changes do not affect the DC bus voltage except for a transient period.
- The SoC of the supercapacitor is automatically controlled to normal value.
- The power exchange algorithm tightly balances the battery SoC. The battery is also protected from DoD and overcharging. In general, the DoD of the battery is correlated with its life cycle [45].
- Since the proposed controller is distributed one, it allows integration of multiple DGs and loads with minor changes in the control loop.
- In the proposed strategy, the supercapacitor is capable to deliver a large power for a very short duration (It is around 5414 watts/second).
- The small-signal model-based controller designing guarantees the stable operation of the DC microgrid.

The structure of this paper is described below. The modeling of the DC microgrid system including ESS devices, constant power load, and resistive load is provided in Section 2. Small-signal modeling of the bidirectional buck-boost converter for ESS is presented in Section 3. The proposed fractional-order voltage shifting controller design for the DC microgrid is detailed in Section 4. RTDS implementation of the proposed controller is discussed in Section 5. Lastly, the contributions and findings are provided in the conclusion Section 6.

2. Modeling of DC microgrid

The DC microgrid considered in this study is shown in Fig. 1. As shown, the battery, the supercapacitor, distributed generator, restive load, and constant power load are connected to the DC bus. All the

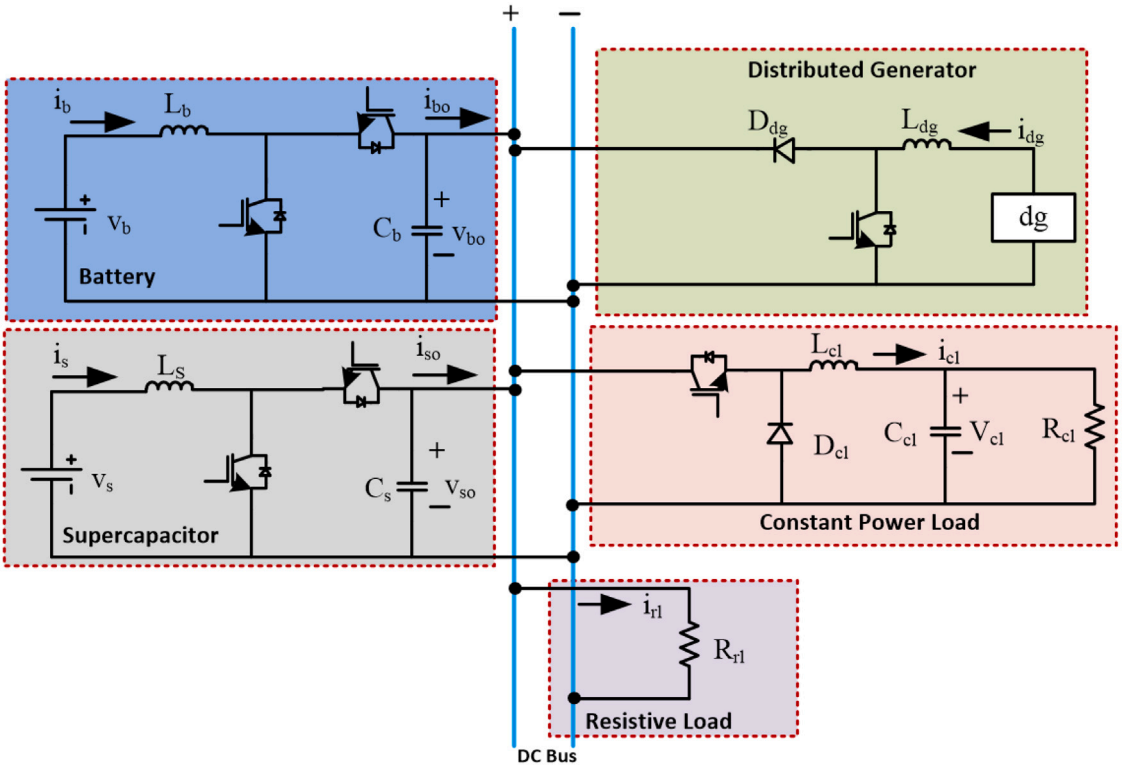

Fig. 1. Connection of sources and loads to the DC bus in the microgrid.

sources and loads are connected to the DC bus through the power electronic converter except the resistive load. The distributed generator meets the power demand for resistive and constant power loads. The battery controller is designed to charge or discharge at steady-state conditions depending on the power imbalance in the DC microgrid. A control design approach is required for the supercapacitor to provide only the fluctuating power. The modeling of the battery, supercapacitor, distributed generator, and constant power load is discussed below.

2.1. Battery and supercapacitor modeling

In this study, the battery and supercapacitor-based hybrid energy storage system is considered. Generally, the battery or supercapacitor is modeled by a series-connected voltage source and impedance where the voltage source is dependent on the state of charge (SoC) of the battery or supercapacitor. The mathematical model of energy storage devices is given below.

$$E_o = E_i(SoC) - I_{es}Z \tag{1}$$

where E_o represents output voltage in volts, E_i is the SoC dependent internal voltage in volts, I_{es} is the energy storage (battery or supercapacitor) devices current in ampere, and Z is the impedance in ohm.

Many complex models can be adopted to calculate the SoC of battery or supercapacitor; however, the simplest method is described by the following equation [46,47].

$$SoC = SoC_i + \frac{1}{C_n}\int I_{es}dt \tag{2}$$

where, SOC_i represents the initial state of charge which is obtained by measurement or provided by the manufacturer, and C_n represents the nominal capacity of the battery or supercapacitor defined by the manufacturer. The charging/discharging efficiency in Eq. (2) is around ~99.9% as reported in the literature [48,49]. In order to avoid complexities, battery and supercapacitor are mostly represented by a series connection of constant voltage source and impedance.

The battery and supercapacitor with rated voltage 200 and 100 V, respectively, are connected to the common DC bus of the DC microgrid through the bidirectional DC-DC converter. Depending on the SoC, the battery or supercapacitor operates either in charging or discharging mode. The battery SoC is managed with the help of DG power control. The DG output power is controlled in such a way that the SoC of the battery is maintained within the limits. If the total power of the DG and battery is unable to meet the load demand, the load-shedding controller is initiated.

2.2. Distributed generator and constant power load modeling

Since this work focuses on fractional-order voltage compensation to stabilize DC bus voltage, any specific technology for distributed generator (DG) is not considered. A DG can be implemented by maximum power point tracking (MPPT) based wind or solar PV system. However, this work considers a generalized model which can mimic the behavior of any renewable energy source. A constant voltage source with a boost controller imitates the behavior of DG as shown in Fig. 1. The power delivered by the DG is controlled by the current command to the boost converter. The conventional proportional-integral (PI) controller is used to regulate the reference current. The interested readers can get more information on DG modeling and converter design in [50].

The constant power load can be implemented by a buck inverter-based resistive load as shown in Fig. 1. A capacitor is connected in parallel to the resistor to maintain a constant voltage. The relationship of the duty cycle of a buck converter and output voltage can be described by the following equation as discussed in [51].

$$G_{cl} = \frac{\tilde{V}_{cl}}{\tilde{D}_{cl}} = \frac{V_{bo}}{L_{cl}C_{cl}s^2 + \frac{L_{cl}}{R_{cl}}s + 1} \tag{3}$$

where $\tilde{V}_{cl}$ and $\tilde{D}_{cl}$ represent voltage across the constant power load and duty cycle, respectively. R_{cl} is a constant resistive load, L_{cl} is the inductance of the constant power load, C_{cl} represents the capacitance of constant power load, V_{bo} represents the battery output voltage.

The conventional PI controller is adopted to process the error between the reference voltage and measured voltage. A DC microgrid can observe DC bus voltage collapse due to inherent negative impedance characteristics of constant power load.

3. Small-signal modeling of bidirectional converter for the proposed controller

In DC microgrid, safe and stable operation can be maintained by properly controlling the energy storage devices. In order to properly design the proposed fractional-order voltage compensation controller for ESS, small-signal model of the non-isolated bidirectional converter is first established. Let us consider the battery storage device part of DC microgrid with the associated bidirectional converter in Fig. 1. The differential equation can be written as below.

$$v_b = L_b \frac{di_b}{dt} + v_{bo}(1-d) \tag{4}$$

$$(1-d)i_b = C_b \frac{dv_{bo}}{dt} + i_{bo} \tag{5}$$

where i_b and v_{bo} are the state variables, and d is the duty of the bidirectional DC-DC converter. Now, linearizing the state variable near the steady-state value, the following equations are obtained.

$$L_b \frac{d\Delta i_b}{dt} = \Delta v_b - (1-D)\Delta v_{bo} + V_{bo}\Delta d \tag{6}$$

$$C_b \frac{d\Delta v_{bo}}{dt} = (1-D)\Delta i_b - I_b \Delta d - \Delta i_{bo} \tag{7}$$

where, terms Δi_b, Δv_b, and Δd represent disturbances in inductor current, battery voltage, and duty cycle. The corresponding steady-state values are I_b, V_b, and D, respectively. The disturbances to the output voltage and current are Δv_{bo}, and Δi_{bo}, respectively. The steady-state values of the output voltage and current are V_{bo}, and I_{bo}, respectively. Now, applying Laplace transformation to Eqs. (6) and (7), the following relationships are derived.

$$G_{vbd} = \frac{\Delta v_{bo}}{\Delta d} = \frac{-LI_b s + (1-D)V_{bo}}{LC_b s^2 + (1-D)^2} \tag{8}$$

$$G_{vib} = \frac{\Delta v_{bo}}{\Delta i_{bo}} = \frac{-Ls}{LC_b s^2 + (1-D)^2} \tag{9}$$

$$G_{ibd} = \frac{\Delta i_{bo}}{\Delta d} = \frac{CV_{bo}s + (1-D)I_b}{LC_b s^2 + (1-D)^2} \tag{10}$$

$$G_{ibd} = \frac{\Delta i_b}{\Delta i_{bo}} = \frac{(1-D)}{LC_b s^2 + (1-D)^2} \tag{11}$$

If the energy conversion loss is ignored, the energy balance between two sides of the bidirectional converter can be written as below.

$$v_b i_b = v_{bo} i_{bo} \tag{12}$$

The small-signal equation can be derived from the above equation by linearizing it around the steady-state value as below.

$$V_b \Delta i_b + I_b \Delta v_b = V_{bo}\Delta i_{bo} + I_{bo}\Delta v_{bo} \tag{13}$$

Applying superposition theorem to Eq. (13), the following relationship is developed.

$$G_{iis} = \frac{\Delta i_b}{\Delta i_{bo}} = \frac{V_{bo}}{V_b} \tag{14}$$

4. The proposed fractional order voltage shifting controller

4.1. Designing the controller

The battery and supercapacitor connection diagram is shown in Fig. 1. Now, considering resistive and capacitive droop strategies for battery and supercapacitor, respectively, the following current sharing equations can be obtained where i_l represents the total load current in the DC microgrid.

$$i_{bo} = \frac{1}{k_d c_v s + 1} i_l \tag{15}$$

$$i_{so} = \frac{k_d c_v s}{k_d c_v s + 1} i_l \tag{16}$$

where, k_d is the battery droop parameter and c_v is the capacitive droop parameter. It is observed that the battery shares only the steady-state part whereas the supercapacitor shares the transient part of the total load current. However, the main problem is that such an approach is unable to minimize the DC bus voltage deviation during load changes or faults in the system. Thus, the fractional voltage term derived from the fractional-order proportional-integral (PI) controller is added to the droop control loop as follows.

$$v_{bo}^* = V_N - i_{bo}k_d + \partial v \tag{17}$$

where, ∂v is the fractional order voltage compensation term derived from error of the DC link voltage and fractional order compensator as below.

$$\partial v = G_f(V_N - v_{bo}) \tag{18}$$

where, G_f represents fractional order compensator which is given by $k_p + \frac{k_i}{s^\lambda}$. V_N is the nominal DC bus voltage, k_p is the proportional gain, k_p is the integral gain, and λ is the fractional order. The interested readers can find details on fractional order controller in the literature [52,53]. Now, the equation can be rewritten as follows.

$$v_{bo}^* = V_N - i_{bo}k_d + G_f(V_N - v_{bo}) \tag{19}$$

Now, linearizing Eq. (19), following equation is obtained.

$$\Delta v_{bo}^* = -k_d \Delta i_{bo} - G_f \Delta v_{bo} \tag{20}$$

The block diagram of the proposed voltage compensation controller for bidirectional DC-DC converter is represented in Fig. 2.

Now, using the small signal model Eqs. (8) to (11), (14), and (20), the small signal model of the proposed controller is obtained as shown in Fig. 3.

From Fig. 3, the small signal closed loop transfer function between Δv_{bo} and Δi_{bo} is obtained as below. The step response of this small-signal model is optimized to obtain the best parameters of the fractional order controller which guarantees stable operations. The detailed optimization process is discussed in the next subsection.

$$tf(s) = \frac{\Delta v_{bo}}{\Delta i_{bo}} = \frac{G_{vid}(1 + G_{bi}G_{ibd}) - (k_d G_{bv} G_{iis} + G_{ibi})G_{bi}G_{vbd}}{(1 + G_{bi}G_{ibd}) + (1 + G_f)G_{bv}G_{iis}G_{bi}G_{vbd}} \tag{21}$$

4.2. Tuning controller parameter

The small-signal transfer function derived from the small-signal model of the proposed controller was presented in the previous subsection. A well know heuristic algorithm, named modified particle swarm optimization (MPSO), is adopted in this subsection to tune the parameters of the proposed fractional-order voltage compensator. This heuristic algorithm is inspired by the sociological behavior of birds flocking [54]. In MPSO, many random particles that move in search space are initially generated to minimize the cost function. MPSO has several advantages such as accurate results with simple operations, faster convergence, and usability for online optimization [55]. For the

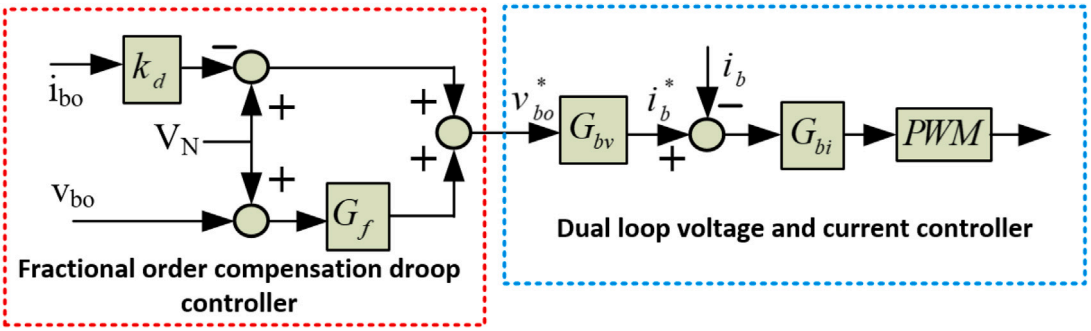

Fig. 2. The proposed fractional order voltage compensation controller.

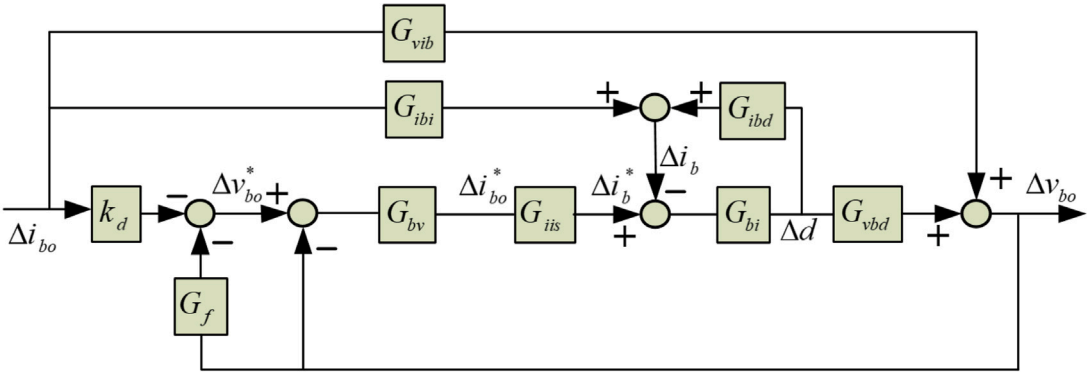

Fig. 3. The small signal model of the proposed controller.

MPSO algorithm, the velocity and position vectors in multi-dimensional space are represented by the following equations [56].

$$v_i^k = c\left\{v_i^{k-1} + c_1 r_1(pb_i^{k-1} - x_i^{k-1}) + c_2 r_2(pb_g^{k-1} - x_i^{k-1})\right\} \tag{22}$$

$$x_i^k = x_i^{k-1} + v_i^k \tag{23}$$

where v_i^k is ith particle velocity in kth, x_i^k is ith particle position in kth iteration; pb_i^{k-1} individual best for ith particle of the $(k-1)$th iteration and pb_g^{k-1} is global best for ith particle of the $(k-1)$; r_1 and r_2 are random numbers in [0 1]; c_1 and c_2 are the learning factors. The constriction factor is derived from the learning factors as below.

$$c = \frac{1}{\left|2 - (c_1 + c_2) - \sqrt{(c_1 + c_2)^2 - 4(c_1 + c_2)}\right|} \tag{24}$$

The maximum and minimum velocity of the particles is calculated from limits as below.

$$v_i^{max,min} = \pm(x_i^{max} - x_i^{min})/N \tag{25}$$

where v_i^{max} is the maximum velocity and v_i^{min} is the minimum velocity of the ith particle; x_i^{max} is the maximum limit and x_i^{min} is the minimum limit of the ith particle; and the number N is generally between the range of 5 to 10. The cost function is defined as below to minimize the integral square error of the step response for the transfer function given by Eq. (21).

$$Minimize: ISE = \int_0^T \Delta e^2 dt \tag{26}$$

$$Variables: k_p, k_i, \lambda \tag{27}$$

$$Constraints: k_{pmin} \le k_p \le k_{pmax}, k_{imin} \le k_i \le k_{imax}, \lambda_{min} \le \lambda \le \lambda_{max} \tag{28}$$

where T is the time of step response and Δe is the error of the step response. The MPSO solution steps are given below to obtain the best value for the fractional-order controller.

Step 1: Initialization of PSO parameters such as population size, number of iterations, learning factors and so on.
Step 2: Calculation of constriction factor, particle velocities, and limits of several variables using Eqs. (24), (25), and (28), respectively. Then, initial population generation within the limits.
Step 3: Running simulation to calculate and minimize objective function described by Eq. (27)
Step 4: Storing the local best and global best
Step 5: Updating the velocity using Eq. (22), and calculation of new population using Eq. (23) from the updated velocities.
Step 6: Checking the stopping criteria. If stopping criteria is not met, returning to step 4.

4.3. Supercapacitor SoC restoration

The supercapacitor state of charge (SoC) is given below.

$$SoC_s = SoC_{sin} + \frac{1}{C_t}\int i_s dt \tag{29}$$

where, SoC_s, SoC_{sin}, C_t, i_s represents supercapacitor SoC, supercapacitor initial SoC, total capacity, and supercapacitor current, respectively. Since the proposed controller is capable to restore DC bus voltage after any load changes or disturbance, the following relation of the voltages can be obtained.

$$V_N = V_{DC} = V_{bo} = V_{so} \tag{30}$$

Considering capacitive droop for supercapacitor and simplifying Eqs. (29) and (30), the following equation can be written.

$$\frac{1}{c_v}\int_{t_b}^{t_r} i_{so} dt = 0 \tag{31}$$

where, c_v, t_b and t_r are the capacitive droop coefficient, beginning time of bus voltage deviation, and bus voltage restoring time, respectively. If the conversion loss of bidirectional converter of the supercapacitor

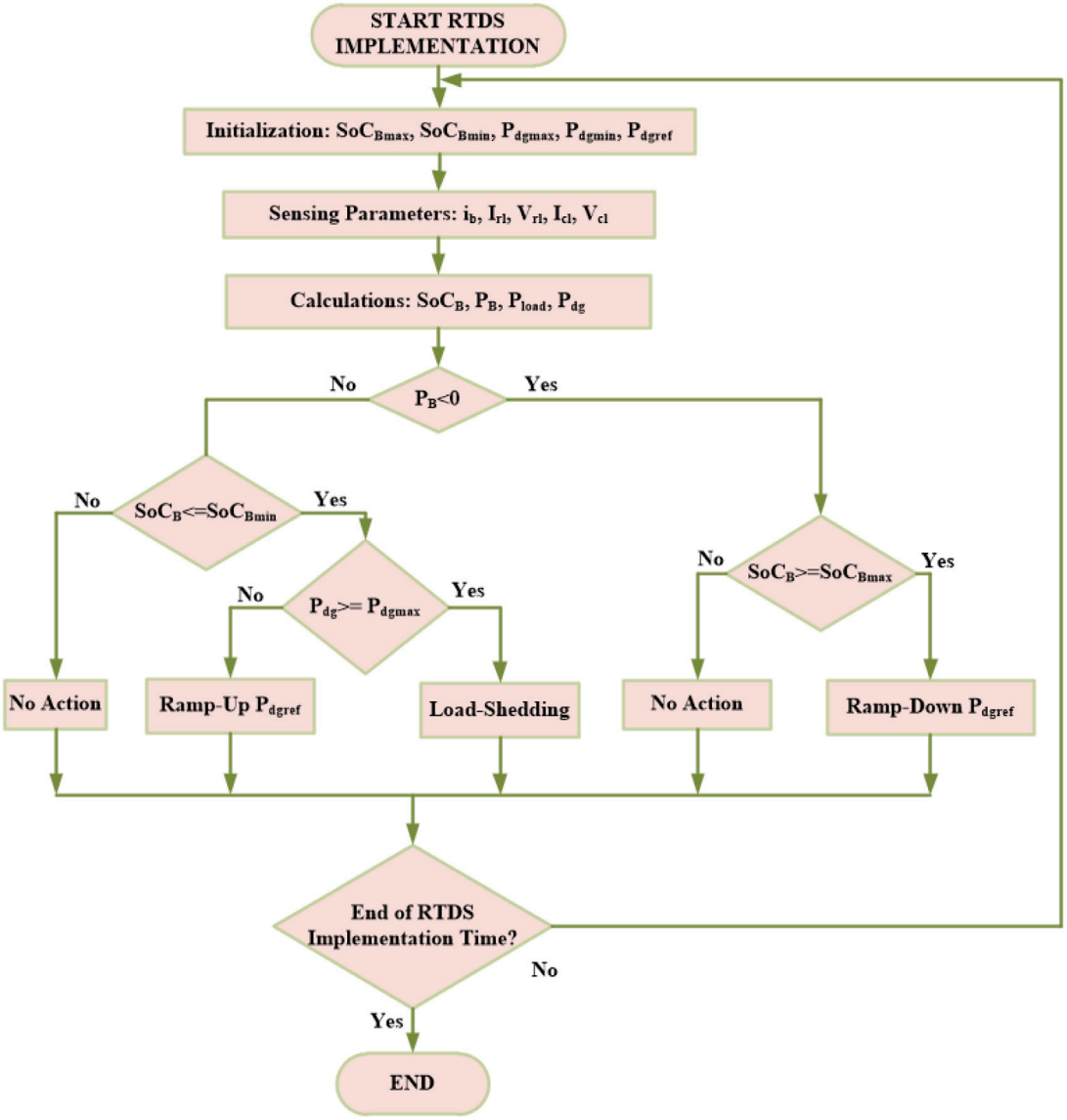

Fig. 4. The battery SoC management algorithm.

is negligible, from the input and output power relationship, i_s can be expressed as

$$i_s = \frac{v_{so} i_{so}}{v_s} \tag{32}$$

Now, simplifying Eqs. (29), (31), and (32), the SoC difference of supercapacitor between the beginning and restoring time of bus voltage deviation is written as

$$SoC_s - SoC_{sin} = \frac{1}{C_t} \int_{t_b}^{t_r} i_s dt = 0 \tag{33}$$

Therefore, the supercapacitor SoC deviation is zero at the end of the bus voltage restoration process. In other words, the proposed control technique is capable to maintain supercapacitor SoC to its initial set point autonomously without any additional controller.

4.4. Battery SoC restoration

The proposed technique is for real-time operation of hybrid energy system in DC microgrid. In real time operation, the battery provides steady-state power for a long time. Thus, the SoC of the battery needs to maintain within the limit in order to improve its life cycle. In this study, the battery SoC is maintained within the limit by desired power delivery from the distributed generator (DG). It is assumed that the DG cam ramp-up or ramp-down the power within its capacity. An rule-based algorithm is developed to balance DC microgrid power depending on the SoC of the battery. The surplus of the DG power is fed to the battery by its controller. If the battery SoC hits the upper limit, the DG power is ramped-down. On the other hand, while the battery SoC nears the lower limit and DG power delivery is at the maximum limit, the load-shedding controller should be initiated. The rule-based SoC management scheme is less complicated and several local measurements can be utilized. This scheme only requires cooperation between battery and DG to balance the SoC. However, optimization-based approach has high computational burden and implementation costs. The detailed rule-based SoC management scheme for the battery is shown in Fig. 4.

5. RTDS implementation results

In this study, the proposed controllers of the DC microgrid are implemented in real time digital simulator (RTDS) platform as shown in Fig. 5. The RTDS can run power system implementation in real-time [57]. This device is fully dedicated to power system simulation and has been widely recognized for designing, developing, and testing

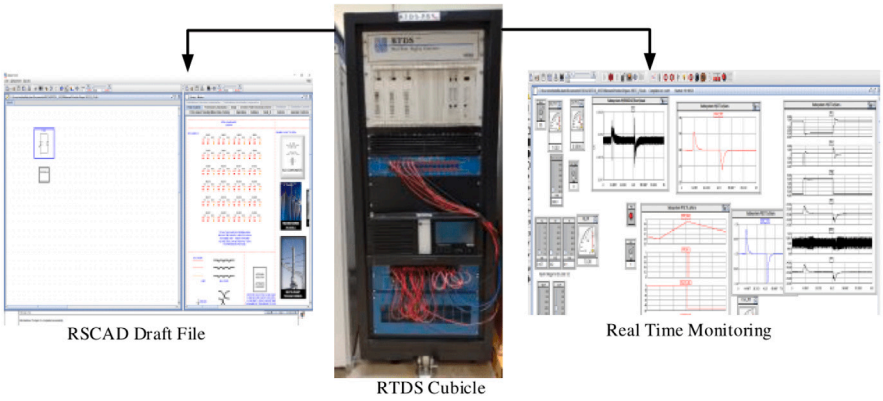

Fig. 5. RTDS setup for DC microgrid implementation.

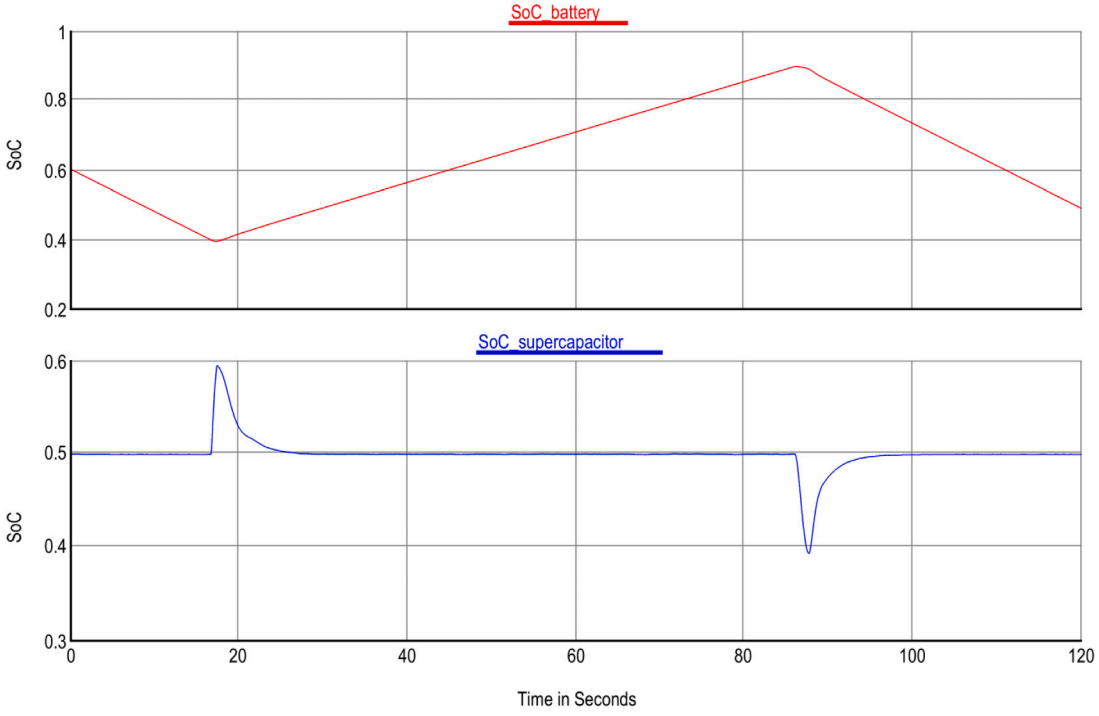

Fig. 6. SoC of battery and supercapacitor.

protection and control systems. The parameters for the DC microgrid and associated controllers are listed in Table 2. Due to high energy density, the battery takes many hours to complete the charging and discharging cycle. So, RTDS takes many hours to provide the results. In this work, in order to get charging/discharging simulation results within several seconds, the charging/discharging parameters were adjusted.

5.1. SoC and power management

The test system with the designed controllers is simulated in RTDS to observe the dynamic performance. The SoC of the supercapacitor and battery is depicted in Fig. 6. The battery SoC is maintained within the limits by proper charging and discharging. While the battery provides load power, it discharges gradually towards the minimum level. The charging or discharging of the battery should be maintained within the lower and upper boundaries to augment the life cycle. The battery power flow is reversed with the power flow algorithm to charge it gradually. Thus, the battery SoC is always properly balanced in the proposed approach. As shown, the battery SoC at around 17 s and 87 s is at the minimum and maximum level, respectively. After these two points, the SoC increases and decreases, respectively, due to the reversal of the battery power.

The SoC of the supercapacitor depends on the process of DC voltage restoration. Since the proposed approach is capable to restore the DC bus voltage quickly after any change in the network, the supercapacitor autonomously maintains its SoC to 0.5 as shown in Fig. 6. DC bus voltage and the power of battery, supercapacitor, and DG are visualized in Fig. 7. In the proposed control approach, the change in load power demand is split into steady-state and transient parts where the battery provides only the steady-state part and the supercapacitor buffers the transient part. As shown in Fig. 7, till 17 s, the system is in the nominal condition, therefore, the supercapacitor provides nearly zero power to the load. On the other hand, in this condition, the load power is provided by the DG and battery. Since the battery gradually discharges, at 17 s, it reaches a lower limit, thus, DG power is ramped up with the proposed algorithm. Since the battery power is reversed at this changing network condition, the supercapacitor buffers the negative large power for a very short duration, and immediately, it settles to zero value. It is visualized that the DC link voltage slightly deviates from

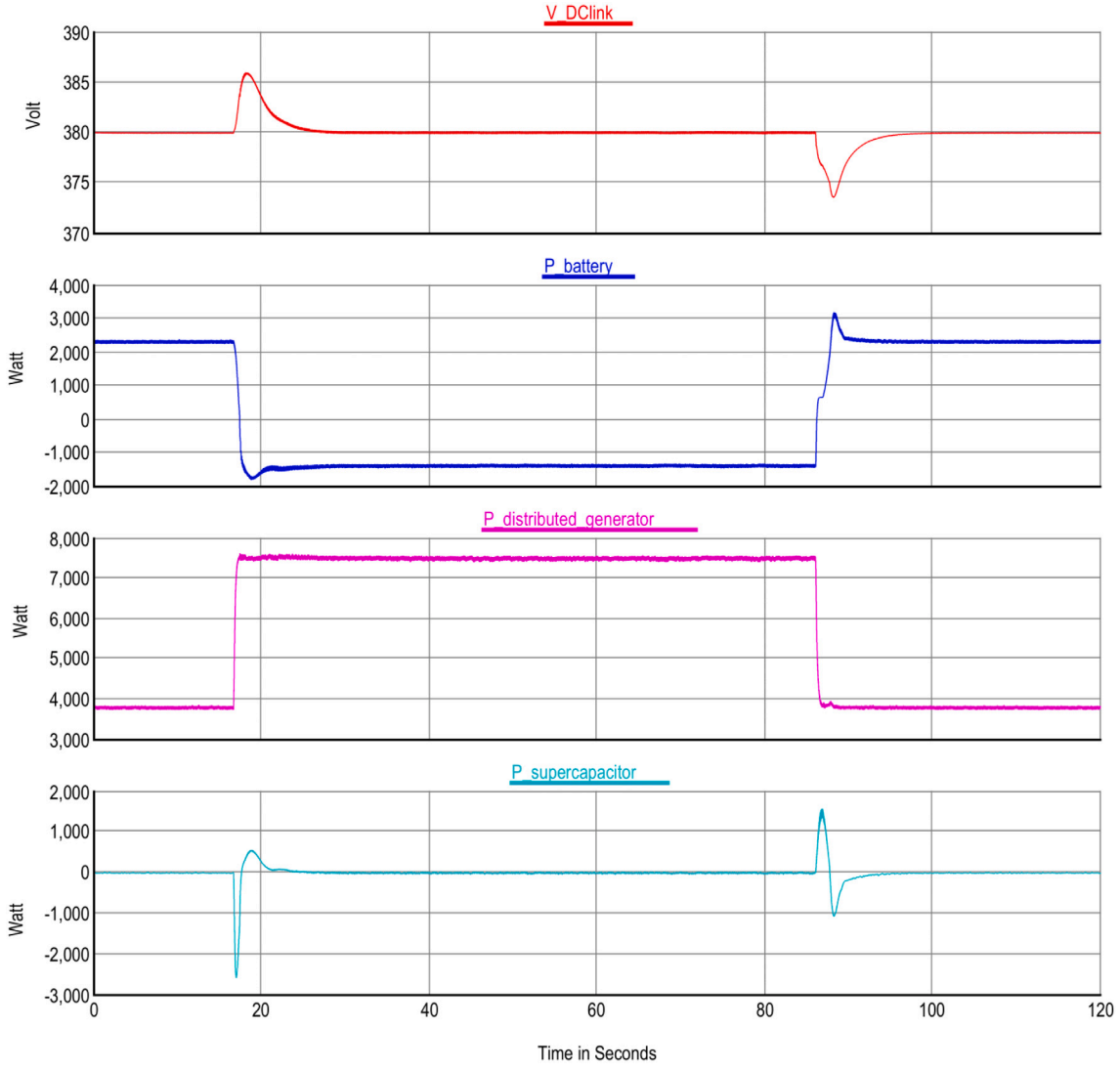

Fig. 7. DC link voltage, battery, DG, and supercapacitor power.

Table 2
DC microgrid and controller parameters.

Symbol	Description	Value
V_b	Battery voltage	200 V
L_b	Battery side inductor	2 mH
C_b	Battery side capacitor	1880 μF
V_s	Supercapacitor voltage	100 V
L_s	Supercapacitor side inductor	2 mH
C_s	Supercapacitor side capacitor	220 μF
V_{dg}	Distributed generator voltage	100 V
L_{dg}	Distributed generator side inductor	1 mH
P_{cl}	Constant power rated power	1.5 kW
V_{cl}	Constant power load side capacitor	2000 μF
G_{bv}	Battery voltage controller transfer function	$(0.0318 + 86.7/s)$
G_{bi}	Battery current controller transfer function	$(0.00069 + 0.657/s)$
G_{sv}	Supercapacitor voltage controller transfer function	$(1.18 + 74.07/s)$
G_{si}	Supercapacitor current controller transfer function	$(0.026 + 20.83/s)$
k_p, k_i, λ	Fractional order controller parameters	0.1, 192, 1.2, respectively

the steady-state value (from 380 V to 386 V). However, it is capable to restore the DC bus voltage quickly due to the action of the fractional-order voltage compensation term in the outer loop of the controller. At around 85 s, the battery power is again revered to protect it from overcharging. At this condition, the DC link voltage slightly decreases from its reference value of 380 V. Then, the DC bus voltage is restored to its preset value which, consequently, helps to regulate supercapacitor SoC. Therefore, the proposed approach is efficient to control the DC bus voltage during the changed network conditions. As shown in Fig. 7, the supercapacitor delivers around 2707 watts power within 0.5 s only. Thus, the power ramping capability of supercapacitor is around 5414 watts per second.

The active power of constant power load (CPL) and resistive load is plotted in Fig. 8. Using a PI controller, the voltage across the CPL

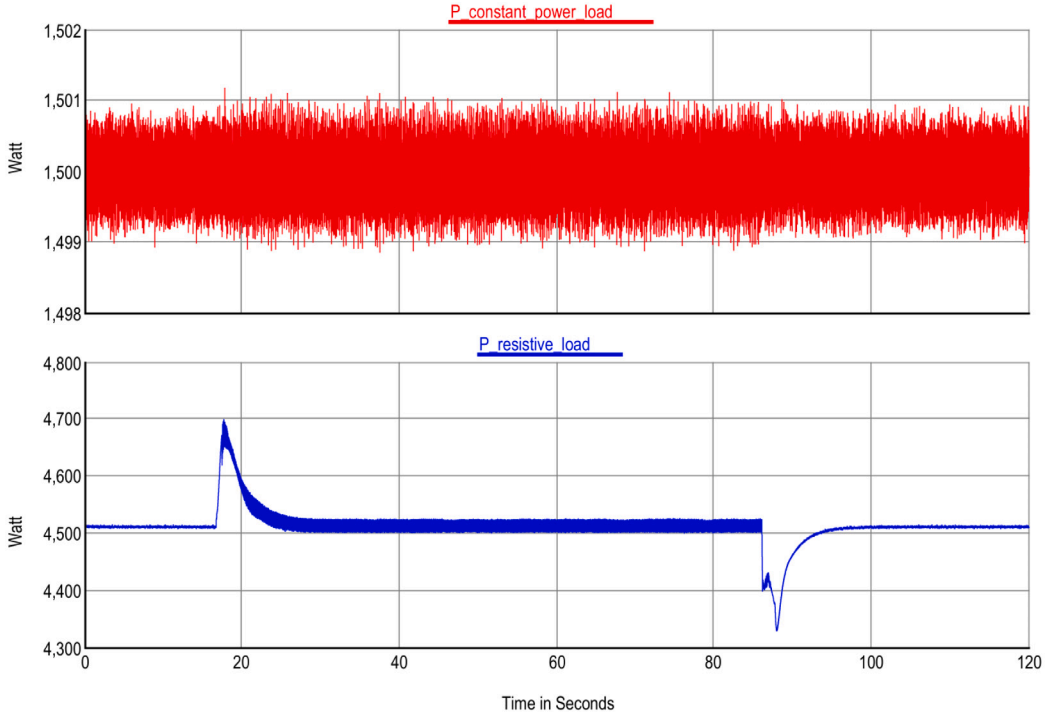

Fig. 8. Constant power and resistive load power.

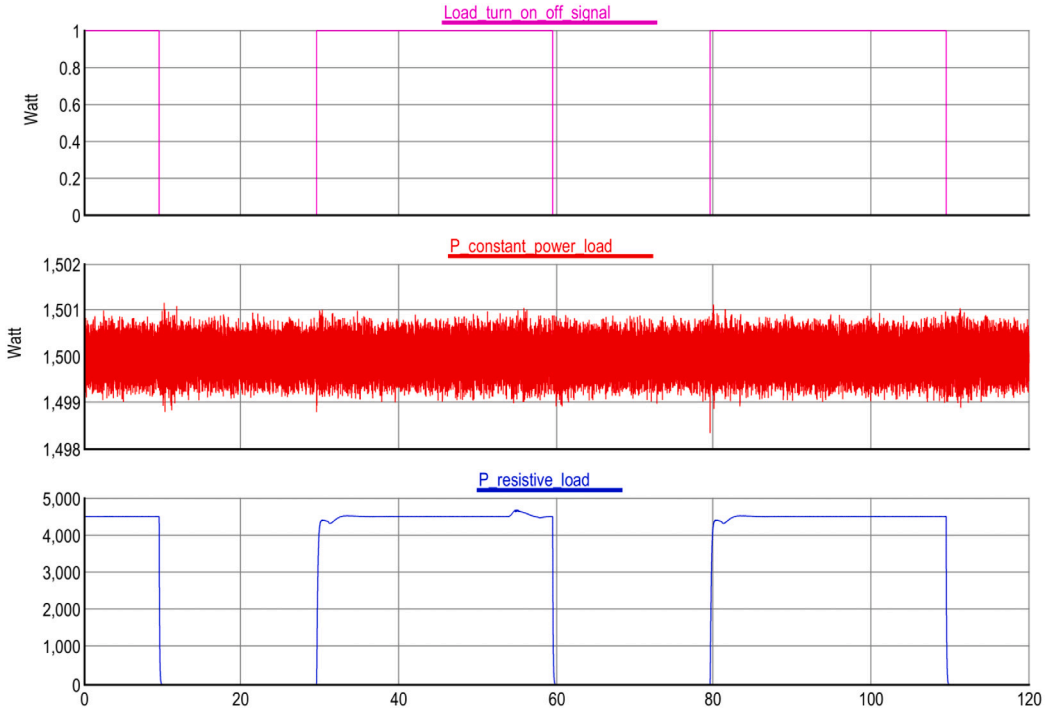

Fig. 9. Load turn on/off signal, constant power, and resistive load power.

is regulated to 127 V. Since the CPL resistor is 9.6 ohm, it always consumes 1500 watts as shown in Fig. 8, which may destabilize the DC microgrid system due to its well-known negative impedance. The proposed control and power management algorithm were capable to stabilize the DC microgrid even with the CPL load. The power of the resistive load follows the transient voltage deviation of the DC link voltage as depicted in Fig. 8.

5.2. Testing pulse loads

The capability of the proposed approach in controlling DC bus voltage, maintaining SoC, and managing active power within the DC microgrid is also tested with pulse loads applied in the DC bus.

The turning on/off signals of resistive load, the active power of resistive load, and CPL are visualized in Fig. 9. As shown, the resistive

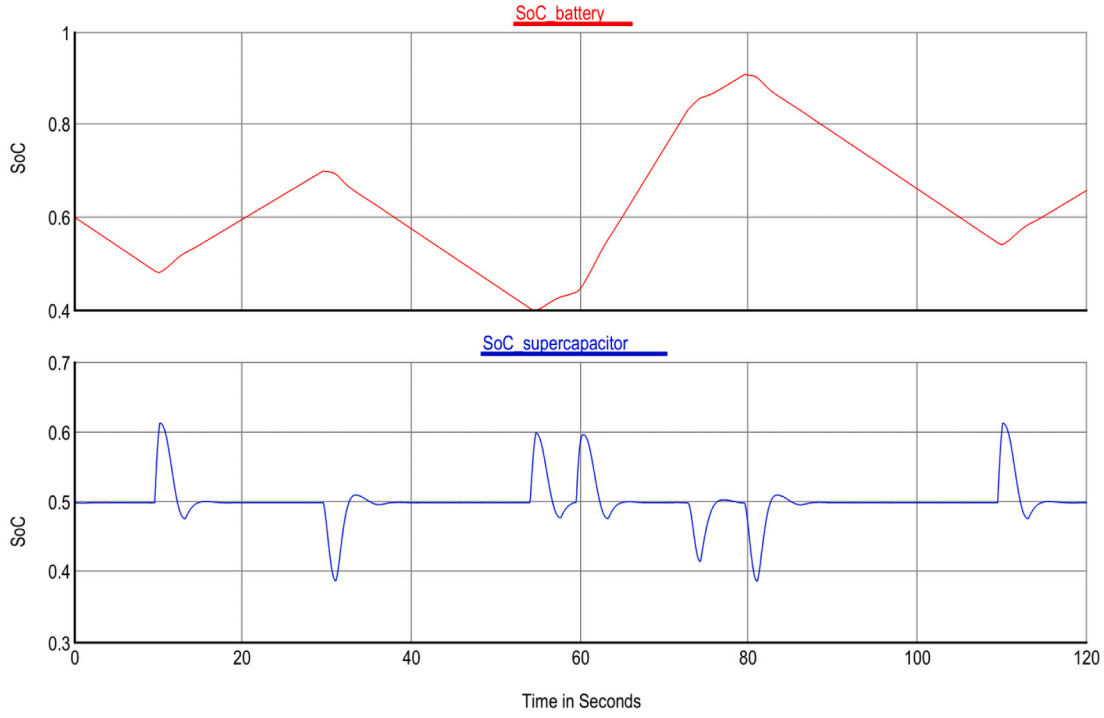

Fig. 10. SoC of battery and supercapacitor under pulse load conditions.

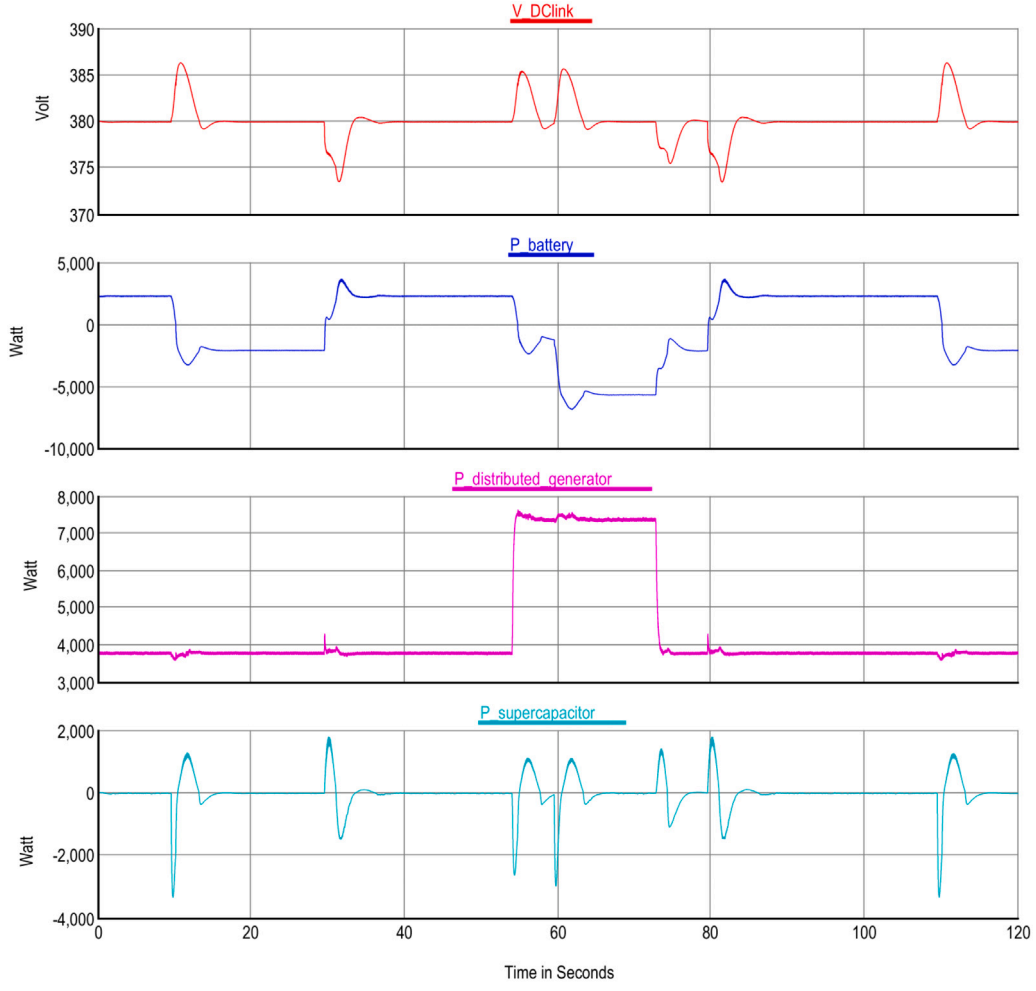

Fig. 11. DC link voltage, battery, DG, and supercapacitor power.

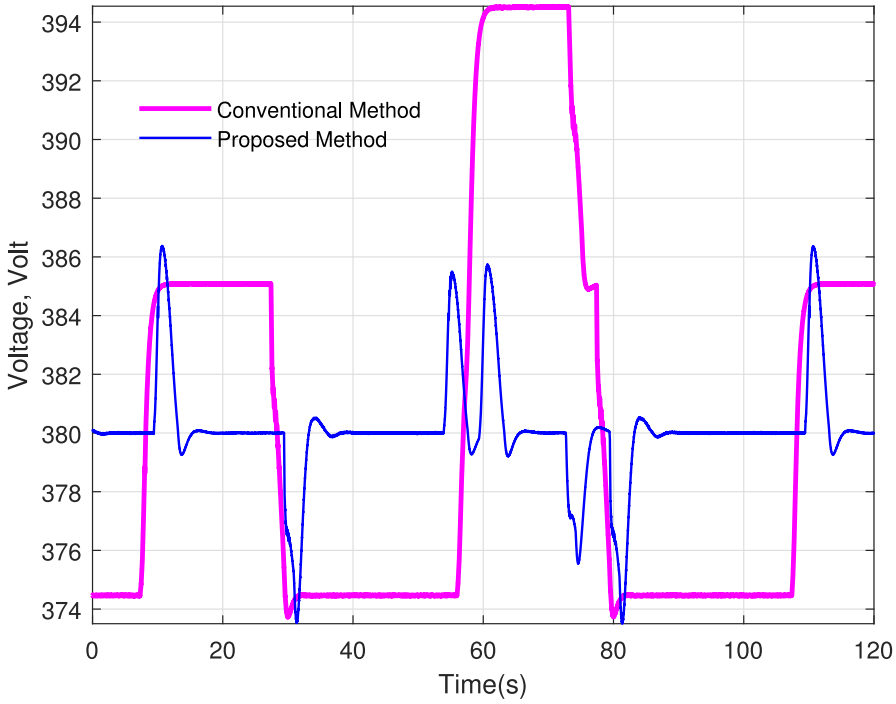

Fig. 12. Comparison of DC link voltage for pulse load tests.

load continuously turns on/off, whereas the CPL consumes 1500 watts during the entire period. The battery and supercapacitor SoC for pulse loads are plotted in Fig. 10. The battery SoC is well maintained within the minimum and maximum limits. The supercapacitor SoC deviates from its initial condition of 0.5 for the transient period only. Thus, the proposed control method is capable to stabilize the DC microgrid during extreme load variation scenarios.

For pulse loads, the DC link voltage, battery power, supercapacitor power, and DG power are visualized in Fig. 11. When the load is turned on or turned off, the positive and negative power demand is effectively split between the battery and the supercapacitor. The battery steady-state power varies between −5800 watts to 2200 watts during multiple load disturbances to properly balance its SoC within the limits.

5.3. Comparative analysis

This section provides a comparative analysis of the proposed compensation mechanism with the conventional approach under pulse loads. The comparative study depicts the superiority of the proposed approach in regulating DC bus voltage as shown in Fig. 12. As shown, the well-known droop controller faces voltage deviation during the entire period due to the connection of constant power load. However, in the proposed fractional-order voltage compensation-based technique, voltage is regulated to a reference value of 380 V efficiently after any pulse loads.

The proposed controller also improves the charging cycle of the battery as depicted in Fig. 13. It is observed that battery charging and discharging cycles start faster in the conventional controller than the proposed controller for most of the cases. For example, the first charging of the battery starts at around 7 s for the conventional controller. However, the charging cycle is delayed to around 9 s with the proposed approach. Likewise first discharging starts at 27.30 s for conventional approach while its start at around 28.90 s for the proposed approach. Therefore, the proposed approach improves the life cycle of the battery. Finally, the comparison of the SoC restoration of the supercapacitor is visualized in Fig. 14. The nominal SoC of the supercapacitor is set to 0.5. Due to the DC bus voltage deviation, the conventional approach is unable to restore the nominal SoC throughout the entire simulation time. However, the proposed voltage compensation mechanism is capable to restore the nominal SoC of the supercapacitor. For example, at around 10 s, the supercapacitor SoC deviates from the nominal value of 0.5 to a new value of 0.62 for a transient period only. It immediately comes back to nominal value. However, the conventional approach is unable to maintain a nominal value in this scenario. In summary, the proposed control and power management schemes provide robust system performance during extreme network conditions. The DC bus voltage, battery charging cycle, and supercapacitor SoC restoration are improved significantly with the proposed voltage compensation mechanism.

6. Conclusions

In this work, a new fractional-order voltage compensation controller has been proposed for islanded DC microgrid. The fractional-order voltage compensation term derived from nominal bus voltage and the battery output voltage is added to the outer control loop of the battery converter. A complete small-signal model is developed for the proposed controller to facilitate parameter tuning. The DC link voltage deviation is reduced for any load changes as compared to the existing approach. The proposed controller guarantees battery life cycle improvement due to the fact that it only provides nominal power. On the other hand, the supercapacitor provides the transient power only, therefore, its SoC is balanced autonomously as the DC bus voltage is restored quickly by fractional-order voltage compensation controller. The battery SoC balancing is achieved with the proficient power-sharing algorithm among DG, loads, and battery. A test case DC microgrid with DG, supercapacitor, battery, resistive and constant power load, and all associated controllers are built in RTDS environment. In the RTDS implementation phase, several load disturbances are executed to show the system performance improvement with the proposed approach. The DC bus voltage, SoC, and active powers are plotted for battery, supercapacitor, DG, and loads. It is found that the proposed approach is capable to reduce the DC voltage deviation as compared to the existing approach in the literature while the supercapacitor SoC is balanced without the need for any additional controller. In the future, the reserve power emulation by PV and wind systems can be implemented to support the SoC balancing of energy storage devices.

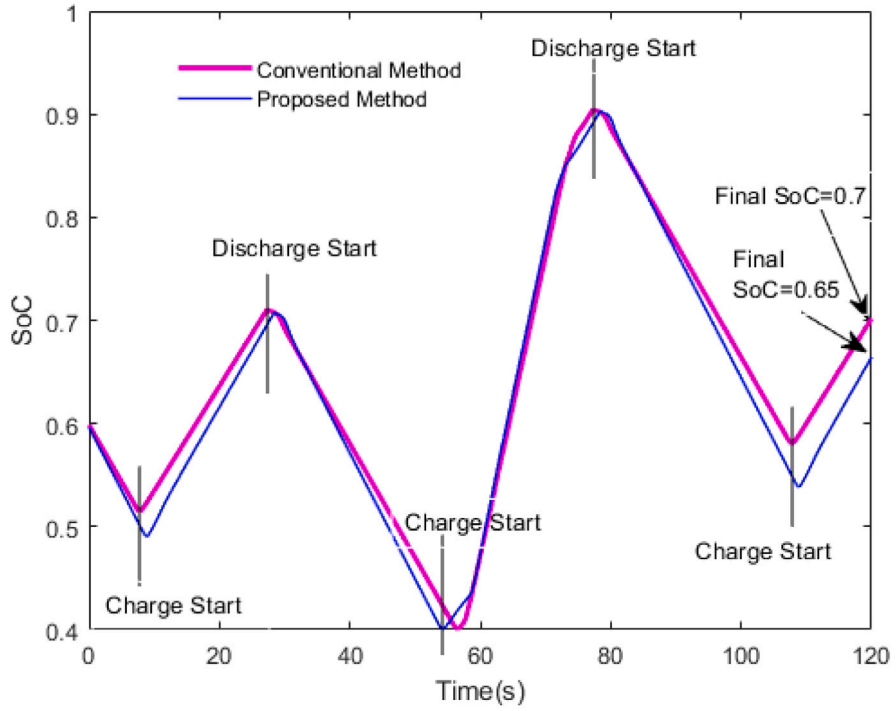

Fig. 13. Comparison of charging and discharging cycle for the battery.

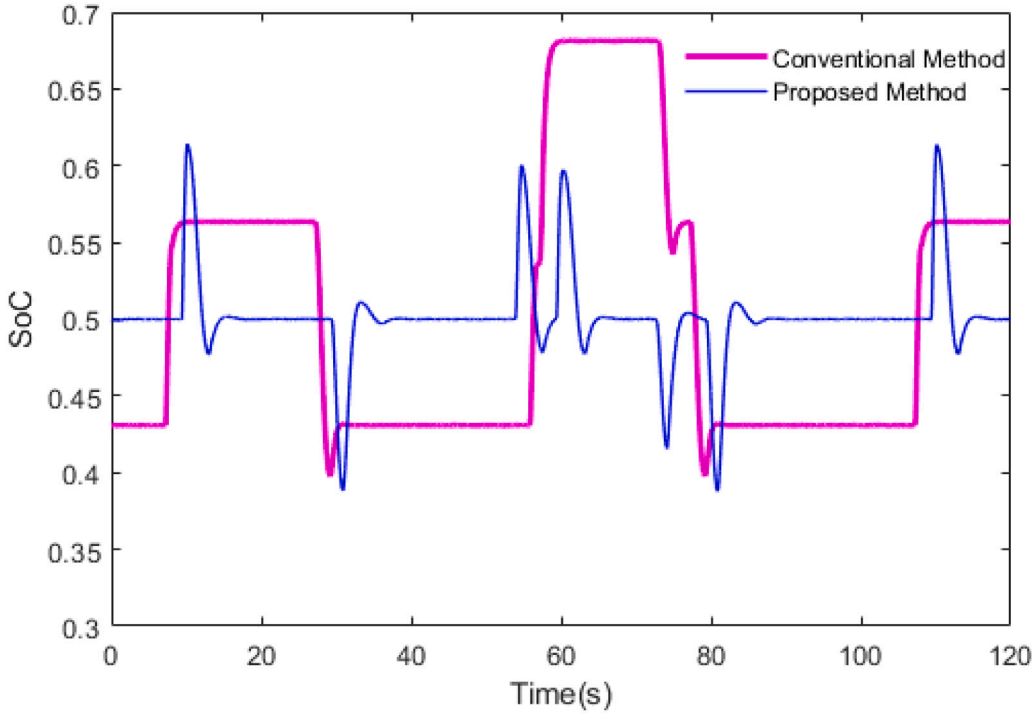

Fig. 14. Comparison of supercapacitor SoC restoration.

CRediT authorship contribution statement

Md. Shafiul Alam: Initiated the conceptual ideas, Designed the methodology, Did the software analysis of the proposed technique, Drafted the manuscript, Improved the manuscript by checking it several times. **Fahad Saleh Al-Ismail:** Verified the proposed control technique, Improved the manuscript by checking it several times. **Fahad A. Al-Sulaiman:** Verified the proposed control technique, Improved the manuscript by checking it several times. **Mohammad. A. Abido:** Designed the methodology, Improved the manuscript by checking it several times.

Declaration of competing interest

The authors declare that they have no known competing financial interests or personal relationships that could have appeared to influence the work reported in this paper.

Data availability

The authors do not have permission to share data.

Acknowledgments

The authors would like to thank King Fahd University of Petroleum & Minerals (KFUPM), Saudi Arabia for its support under Direct Funded Project No. DF201022. The authors also acknowledge the support provided by ARCEMS, IRC-REPS, and KACARE ERIC, KFUPM, Saudi Arabia.

References

[1] M.S. Alam, F.S. Al-Ismail, A. Salem, M.A. Abido, High-level penetration of renewable energy sources into grid utility: Challenges and solutions, IEEE Access 8 (2020) 190277–190299.
[2] H. Saberi, H. Nazaripouya, S. Mehraeen, Implementation of a stable solar-powered microgrid testbed for remote applications, Sustainability 13 (5) (2021) 2707.
[3] A. El-Shahat, S. Sumaiya, DC-microgrid system design, control, and analysis, Electronics 8 (2) (2019) 124.
[4] H.A. Alsiraji, R. El-Shatshat, Virtual synchronous machine/dual-droop controller for parallel interlinking converters in hybrid AC–DC microgrids, Arab. J. Sci. Eng. 46 (2) (2021) 983–1000.
[5] X.-K. Liu, Y.-W. Wang, P. Lin, P. Wang, Distributed supervisory secondary control for a DC microgrid, IEEE Trans. Energy Convers. 35 (4) (2020) 1736–1746.
[6] L. Meng, Q. Shafiee, G.F. Trecate, H. Karimi, D. Fulwani, X. Lu, J.M. Guerrero, Review on control of DC microgrids and multiple microgrid clusters, IEEE J. Emerg. Sel. Top. Power Electron. 5 (3) (2017) 928–948.
[7] F. Gao, S. Bozhko, A. Costabeber, C. Patel, P. Wheeler, C.I. Hill, G. Asher, Comparative stability analysis of droop control approaches in voltage-source-converter-based DC microgrids, IEEE Trans. Power Electron. 32 (3) (2016) 2395–2415.
[8] P. Prabhakaran, Y. Goyal, V. Agarwal, Novel nonlinear droop control techniques to overcome the load sharing and voltage regulation issues in DC microgrid, IEEE Trans. Power Electron. 33 (5) (2017) 4477–4487.
[9] X.-K. Liu, H. He, Y.-W. Wang, Q. Xu, F. Guo, Distributed hybrid secondary control for a DC microgrid via discrete-time interaction, IEEE Trans. Energy Convers. 33 (4) (2018) 1865–1875.
[10] I. Zafeiratou, I. Prodan, L. Lefèvre, L. Piétrac, Meshed DC microgrid hierarchical control: A differential flatness approach, Electr. Power Syst. Res. 180 (2020) 106133.
[11] M. Yuan, Y. Fu, Y. Mi, Z. Li, C. Wang, Hierarchical control of DC microgrid with dynamical load power sharing, Appl. Energy 239 (2019) 1–11.
[12] A.A. Mohamed, A.T. Elsayed, T.A. Youssef, O.A. Mohammed, Hierarchical control for DC microgrid clusters with high penetration of distributed energy resources, Electr. Power Syst. Res. 148 (2017) 210–219.
[13] J.M. Guerrero, J.C. Vasquez, J. Matas, L.G. De Vicuña, M. Castilla, Hierarchical control of droop-controlled AC and DC microgrids—A general approach toward standardization, IEEE Trans. Ind. Electron. 58 (1) (2010) 158–172.
[14] P. Lin, C. Zhang, J. Wang, C. Jin, P. Wang, On autonomous large-signal stabilization for islanded multibus DC microgrids: A uniform nonsmooth control scheme, IEEE Trans. Ind. Electron. 67 (6) (2019) 4600–4612.
[15] S. Wang, M. Du, L. Lu, W. Xing, K. Sun, M. Ouyang, Multi-level energy management of a DC microgrid based on virtual-battery model considering voltage regulation and economic optimization, IEEE J. Emerg. Sel. Top. Power Electron. (2020).
[16] V. Nasirian, A. Davoudi, F.L. Lewis, J.M. Guerrero, Distributed adaptive droop control for DC distribution systems, IEEE Trans. Energy Convers. 29 (4) (2014) 944–956.
[17] Y. Sun, X. Wu, J. Wang, D. Hou, S. Wang, Power compensation of network losses in a microgrid with BESS by distributed consensus algorithm, IEEE Trans. Syst. Man Cybern.: Syst. 51 (4) (2020) 2091–2100.
[18] X. Kong, X. Liu, L. Ma, K.Y. Lee, Hierarchical distributed model predictive control of standalone wind/solar/battery power system, IEEE Trans. Syst. Man Cybern.: Syst. 49 (8) (2019) 1570–1581.
[19] P.B. Nempu, J.N. Sabhahit, Stochastic algorithms for controller optimization of grid tied hybrid AC/DC microgrid with multiple renewable sources, Adv. Electr. Comput. Eng. 19 (2) (2019) 53–60.
[20] Y. Wang, L. Wang, M. Li, Z. Chen, A review of key issues for control and management in battery and ultra-capacitor hybrid energy storage systems, ETransportation 4 (2020) 100064.
[21] Y. Sahri, Y. Belkhier, S. Tamalouzt, N. Ullah, R.N. Shaw, M. Chowdhury, K. Techato, et al., Energy management system for hybrid PV/Wind/Battery/Fuel cell in microgrid-based hydrogen and economical hybrid battery/super capacitor energy storage, Energies 14 (18) (2021) 5722.
[22] M.A. Zabara, C.B. Uzundal, B. Ülgüt, Performance modeling of unmanaged hybrid battery/supercapacitor energy storage systems, J. Energy Storage 43 (2021) 103185.
[23] S. Vasantharaj, V. Indragandhi, V. Subramaniyaswamy, Y. Teekaraman, R. Kuppusamy, S. Nikolovski, Efficient control of DC microgrid with hybrid PV—Fuel cell and energy storage systems, Energies 14 (11) (2021) 3234.
[24] Q. Zhang, L. Wang, G. Li, Y. Liu, A real-time energy management control strategy for battery and supercapacitor hybrid energy storage systems of pure electric vehicles, J. Energy Storage 31 (2020) 101721.
[25] B. Liu, F. Zhuo, Y. Zhu, H. Yi, System operation and energy management of a renewable energy-based DC micro-grid for high penetration depth application, IEEE Trans. Smart Grid 6 (3) (2014) 1147–1155.
[26] J. Xiao, P. Wang, L. Setyawan, Q. Xu, Multi-level energy management system for real-time scheduling of DC microgrids with multiple slack terminals, IEEE Trans. Energy Convers. 31 (1) (2015) 392–400.
[27] X. Lu, J.M. Guerrero, K. Sun, J.C. Vasquez, An improved droop control method for DC microgrids based on low bandwidth communication with DC bus voltage restoration and enhanced current sharing accuracy, IEEE Trans. Power Electron. 29 (4) (2013) 1800–1812.
[28] Q. Xu, J. Xiao, X. Hu, P. Wang, M.Y. Lee, A decentralized power management strategy for hybrid energy storage system with autonomous bus voltage restoration and state-of-charge recovery, IEEE Trans. Ind. Electron. 64 (9) (2017) 7098–7108.
[29] S.N. Motapon, L.-A. Dessaint, K. Al-Haddad, A robust H2-consumption-minimization-based energy management strategy for a fuel cell hybrid emergency power system of more electric aircraft, IEEE Trans. Ind. Electron. 61 (11) (2014) 6148–6156.
[30] J. Shen, A. Khaligh, A supervisory energy management control strategy in a battery/ultracapacitor hybrid energy storage system, IEEE Trans. Transp. Electr. 1 (3) (2015) 223–231.
[31] B. Hredzak, V.G. Agelidis, M. Jang, A model predictive control system for a hybrid battery-ultracapacitor power source, IEEE Trans. Power Electron. 29 (3) (2013) 1469–1479.
[32] Y. Shan, J. Hu, K.W. Chan, Q. Fu, J.M. Guerrero, Model predictive control of bidirectional DC–DC converters and AC/DC interlinking converters—A new control method for PV-wind-battery microgrids, IEEE Trans. Sustain. Energy 10 (4) (2018) 1823–1833.
[33] W. Wang, M. Zhou, H. Jiang, Z. Chen, Q. Wang, Improved droop control based on state-of-charge in DC microgrid, in: 2020 IEEE 29th International Symposium on Industrial Electronics, ISIE, IEEE, 2020, pp. 1509–1513.
[34] Z. Peng, J. Wang, D. Bi, Y. Wen, Y. Dai, X. Yin, Z.J. Shen, Droop control strategy incorporating coupling compensation and virtual impedance for microgrid application, IEEE Trans. Energy Convers. 34 (1) (2019) 277–291.
[35] M.S. Alam, F.S. Al-Ismail, M.A. Abido, Power management and state of charge restoration of direct current microgrid with improved voltage-shifting controller, J. Energy Storage 44 (2021) 103253.
[36] Z. Wang, P. Wang, W. Jiang, P. Wang, A decentralized automatic load power allocation strategy for hybrid energy storage system, IEEE Trans. Energy Convers. (2020).
[37] Q. Xu, X. Hu, P. Wang, J. Xiao, P. Tu, C. Wen, M.Y. Lee, A decentralized dynamic power sharing strategy for hybrid energy storage system in autonomous DC microgrid, IEEE Trans. Ind. Electron. 64 (7) (2016) 5930–5941.
[38] R. Zhang, B. Hredzak, T. Morstyn, Distributed control with virtual capacitance for the voltage restorations, state of charge balancing, and load allocations of heterogeneous energy storages in a DC datacenter microgrid, IEEE Trans. Energy Convers. 34 (3) (2018) 1296–1308.
[39] E.K. Belal, D.M. Yehia, A.M. Azmy, Adaptive droop control for balancing SOC of distributed batteries in DC microgrids, IET Gener. Transm. Distrib. 13 (20) (2019) 4667–4676.
[40] E. Espina, J. Llanos, C. Burgos-Mellado, R. Cardenas-Dobson, M. Martinez-Gomez, D. Sáez, Distributed control strategies for microgrids: An overview, IEEE Access 8 (2020) 193412–193448.
[41] Y. Wang, S. Mondal, K. Satpathi, Y. Xu, S. Dasgupta, A.K. Gupta, Multiagent distributed power management of DC shipboard power systems for optimal fuel efficiency, IEEE Trans. Transp. Electr. 7 (4) (2021) 3050–3061.
[42] C. Papadimitriou, E. Zountouridou, N. Hatziargyriou, Review of hierarchical control in DC microgrids, Electr. Power Syst. Res. 122 (2015) 159–167.
[43] P. Lin, T. Zhao, B. Wang, Y. Wang, P. Wang, A semi-consensus strategy toward multi-functional hybrid energy storage system in DC microgrids, IEEE Trans. Energy Convers. 35 (1) (2019) 336–346.
[44] E.J. Smith, D.A. Robinson, A.P. Agalgaonkar, A secondary strategy for unbalance consensus in an islanded voltage source converter-based microgrid using cooperative gain control, Electr. Power Syst. Res. 210 (2022) 108097.
[45] S. Xie, S. Qi, K. Lang, A data-driven power management strategy for plug-in hybrid electric vehicles including optimal battery depth of discharging, IEEE Trans. Ind. Inf. 16 (5) (2019) 3387–3396.
[46] M.A. Hannan, M.H. Lipu, A. Hussain, A. Mohamed, A review of lithium-ion battery state of charge estimation and management system in electric vehicle applications: Challenges and recommendations, Renew. Sustain. Energy Rev. 78 (2017) 834–854.

[47] R. Xiong, J. Cao, Q. Yu, H. He, F. Sun, Critical review on the battery state of charge estimation methods for electric vehicles, Ieee Access 6 (2017) 1832–1843.
[48] A. Smith, J. Burns, J. Dahn, A high precision study of the Coulombic efficiency of Li-ion batteries, Electrochem. Solid-State Lett. 13 (12) (2010) A177.
[49] R. Wang, C. Song, W. Huang, J. Zhao, Improvement of battery pack efficiency and battery equalization based on the extremum seeking control, Int. J. Electr. Power Energy Syst. 137 (2022) 107829.
[50] P.J. dos Santos Neto, T.A. dos Santos Barros, J.P.C. Silveira, E. Ruppert Filho, J.C. Vasquez, J.M. Guerrero, Power management strategy based on virtual inertia for DC microgrids, IEEE Trans. Power Electron. (2020).
[51] F. Blaabjerg, Control of Power Electronic Converters and Systems: Vol. 2, Academic Press, 2018.
[52] I. Podlubny, Fractional-order systems and $PI^{\lambda}D^{\mu}$ controllers, IEEE Trans. Automat. Control 44 (1) (1999) 208–214.
[53] H. Li, Y. Luo, Y. Chen, A fractional order proportional and derivative (FOPD) motion controller: Tuning rule and experiments, IEEE Trans. Control Syst. Technol. 18 (2) (2009) 516–520.
[54] M. Abido, Optimal design of power-system stabilizers using particle swarm optimization, IEEE Trans. Energy Convers. 17 (3) (2002) 406–413.
[55] M.S. Alam, F.S. Al-Ismail, M.A. Abido, PV/Wind-Integrated low-inertia system frequency control: PSO-optimized fractional-order PI-based SMES approach, Sustainability 13 (14) (2021) 7622.
[56] M.A. Hossain, H.R. Pota, S. Squartini, A.F. Abdou, Modified PSO algorithm for real-time energy management in grid-connected microgrids, Renew. Energy 136 (2019) 746–757.
[57] M.S. Alam, M.J. Rana, M. Abido, Real time digital simulation of voltage source converter controller for HVDC application, in: 2017 9th IEEE-GCC Conference and Exhibition, GCCCE, IEEE, 2017, pp. 1–9.